

Five transiting hot Jupiters discovered using WASP-South, Euler and TRAPPIST: WASP-119 b, WASP-124 b, WASP-126 b, WASP-129 b and WASP-133 b [★]

P. F. L. Maxted¹, D. R. Anderson¹, A. Collier Cameron², L. Delrez³, M. Gillon³, C. Hellier¹, E. Jehin³, M. Lendl^{4,5}, M. Neveu-VanMalle^{5,6}, F. Pepe⁵, D. Pollacco⁷, D. Queloz^{6,5}, D. Ségransan⁵, B. Smalley¹, A. M. S. Smith^{1,8}, J. Southworth¹, A. H. M. J. Triaud^{5,9,10}, S. Udry⁵, T. Wagg¹, and R. G. West⁷

¹ Astrophysics Group, Keele University, Staffordshire, ST5 5BG, UK e-mail: p.maxted@keele.ac.uk

² SUPA, School of Physics and Astronomy, University of St. Andrews, North Haugh, Fife, KY16 9SS, UK

³ Institut d'Astrophysique et de Géophysique, Université de Liège, Allée du 6 Août, 17, Bat. B5C, Liège 1, Belgium

⁴ Space Research Institute, Austrian Academy of Sciences, Schmiedlstr. 6, 8042 Graz, Austria

⁵ Observatoire astronomique de l'Université de Genève 51 ch. des Maillettes, 1290 Sauverny, Switzerland

⁶ Cavendish Laboratory, J J Thomson Avenue, Cambridge, CB3 0HE, UK

⁷ Department of Physics, University of Warwick, Coventry CV4 7AL, UK

⁸ Institute of Planetary Research, German Aerospace Center, Rutherfordstrasse 2, 12489 Berlin, Germany

⁹ Centre for Planetary Sciences, University of Toronto at Scarborough, 1265 Military Trail, Toronto, ON, M1C 1A4, Canada

¹⁰ Department of Astronomy & Astrophysics, University of Toronto, Toronto, ON, M5S 3H4, Canada

April 28, 2016

ABSTRACT

We have used photometry from the WASP-South instrument to identify 5 stars showing planet-like transits in their light curves. The planetary nature of the companions to these stars has been confirmed using photometry from the EulerCam instrument on the Swiss Euler 1.2-m telescope and the TRAPPIST telescope, and spectroscopy obtained with the CORALIE spectrograph. The planets discovered are hot Jupiter systems with orbital periods in the range 2.17 to 5.75 days, masses from $0.3 M_{\text{Jup}}$ to $1.2 M_{\text{Jup}}$ and with radii from $1 R_{\text{Jup}}$ to $1.5 R_{\text{Jup}}$. These planets orbit bright stars ($V = 11 - 13$) with spectral types in the range F9 to G4. WASP-126 is the brightest planetary system in this sample and hosts a low-mass planet with a large radius ($0.3 M_{\text{Jup}}$, $0.95 R_{\text{Jup}}$), making it a good target for transmission spectroscopy. The high density of WASP-129 A suggests that it is a helium-rich star similar to HAT-P-11 A. WASP-133 A has an enhanced surface lithium abundance compared to other old G-type stars, particularly other planet host stars. These planetary systems are good targets for follow-up observations with ground-based and space-based facilities to study their atmospheric and dynamical properties.

Key words. planetary systems

1. Introduction

Ground-based transit surveys such as WASP (Pollacco et al. 2008), HAT (Bakos et al. 2004), HAT-South (Bakos et al. 2013) and KELT (Pepper et al. 2008) have identified the majority of bright hot Jupiter planetary systems that have been studied in detail using observations with large ground-based telescopes and space-based instrumentation. Although space-based surveys such as Kepler-K2 (Howell et al. 2014), TESS (Ricker et al. 2015) and PLATO (Rauer et al. 2014) will produce much higher quality photometry than is possible from the ground, it is advantageous to identify as many planetary systems as possible in the areas of the sky that will be observed by these missions so that the observing strategy can be optimised. This was clearly demonstrated by the recent discovery that WASP-47 is a very rare example of a multiple-planet system containing a hot Jupiter (Becker et al. 2015; Neveu-VanMalle et al. 2015). This discovery was only possible because this known planetary system was

prioritised for high-cadence observations with Kepler-K2. These high-cadence observations made it possible to detect the transit time variations produced by the gravitational interactions between the planets in this system. The discovery that WASP-47 is a multi-planet system also demonstrates that detailed observations of apparently normal hot Jupiter systems continue to reveal unexpected properties of this diverse group of planetary systems.

Here we present the discovery of 5 hot-Jupiter planetary systems in the southern hemisphere. Section 2 describes the observations we have obtained, section 3 describes our analysis of the host stars, the stellar and planetary masses and radii are derived in section 4 and we discuss the properties of each system briefly in section 5.

2. Observations

WASP-South uses an array of 8 cameras that observe selected regions of the southern sky with a combined area of approximately 450 square degrees at a typical cadence of about 8 minutes and the exposure time is 30 s. The WASP survey and instruments are described in Pollacco et al. (2006) and a description of our

[★] The photometric data and radial velocity measurements used in this study are available at the CDS via anonymous ftp to cdsarc.u-strasbg.fr (130.79.128.5) or via <http://cdsweb.u-strasbg.fr/cgi-bin/qcat?J/A+A/>.

Table 2. Light curves of five transiting exoplanet systems. This table is available in its entirety at CDS. The first few lines are shown here for guidance as to its contents and format. Column 1 is the WASP identification number of the star. Column 2 indicates the source of the observation as follows: W – WASP-South; T – TRAPPIST; E – EulerCam. Column 3 indicates the filter used for the observations as follows: WASP – 400 – 700 nm; NIR – Astrodon NIR 700 nm cut-on luminance; Exo – Astrodon ExoPlanet-BB; NGTS – EulerCam NGTS; $z_p - z'$; Gunn – Gunn R; I_C – Cousins I_C. Column 4 is the UTC date of the observation given as HJD-2450000. Columns 5 and 6 are the apparent magnitude of the star and its standard error relative to the mean out-of-transit apparent magnitude. Column 7 is a flag that is set to the value 1 for the first observation after a meridian flip with the TRAPPIST telescope.

WASP-	Source	Filter	Date	Δm	σ_m	Flip
119	W	WASP	5780.52513	0.0123	0.0163	0
119	W	WASP	5780.52557	-0.0135	0.0159	0
119	W	WASP	5780.54147	-0.0014	0.0156	0

Table 1. Log of observations. Data obtained after an upgrade to the CORALIE spectrograph in November 2014 are treated separately to data obtained before the upgrade. In the final column we list either the number of observations obtained with WASP-South, or the number of spectra obtained, or the filter used to obtained the transit photometry. The different filters used are described in the text.

Facility	Date	Notes
WASP-119		
WASP-South	2010 Aug – 2012 Feb	14 010 points
CORALIE	2013 Sep–2014 Nov	18 spectra
CORALIE	2015 Jan–2015 Sep	5 spectra
TRAPPIST	2013 Nov 15	NIR
WASP-124		
WASP-South	2006 May – 2011 Nov	15 165 points
CORALIE	2011 Dec – 2014 Oct	28 spectra
CORALIE	2015 May – 2015 Nov	13 spectra
TRAPPIST	2012 Nov 17	ExoPlanet-BB
TRAPPIST	2013 May 28	ExoPlanet-BB
TRAPPIST	2013 Jun 07	ExoPlanet-BB
TRAPPIST	2013 Aug 17	ExoPlanet-BB
TRAPPIST	2013 Nov 06	ExoPlanet-BB
Euler	2015 Jul 16	NGTS filter
WASP-126		
WASP-South	2010 Aug–2012 Feb	13 245 points
CORALIE	2013 Oct–2014 Oct	22 spectra
CORALIE	2014 Nov–2015 Sep	8 spectra
TRAPPIST	2014 Jan 08	z'
TRAPPIST	2014 Jan 31	z'
Euler	2014 Sep 05	Gunn r filter
Euler	2014 Oct 17	Gunn r filter
Euler	2014 Nov 06	Gunn r filter
WASP-129		
WASP-South	2006 May–2012 May	26 940 points
CORALIE	2014 Feb–2014 Jun	9 spectra
Euler	2015 Mar 08	NGTS filter
Euler	2015 Mar 31	I _C
TRAPPIST	2015 Mar 31	NIR
WASP-133		
WASP-South	2006 May–2012 Jun	18 436 points
CORALIE	2014 Aug–2014 Oct	12 spectra
TRAPPIST	2014 Sep 26	ExoPlanet-BB
Euler	2015 Jun 14	NGTS filter
TRAPPIST	2015 Aug 25	ExoPlanet-BB

planet-hunting methods can be found in Pollacco et al. (2008) and Collier Cameron et al. (2007).

WASP-South planet candidates are followed up using the TRAPPIST robotic photometer (Jehin et al. 2011; Gillon et al.

Table 3. CORALIE radial velocities. This table is available in its entirety at CDS. The first few lines are shown here for guidance as to its contents and format. Data are provided to the full precision used for calculations, but times of mid-exposure are only accurate to a few minutes. The standard error on the bisector span (BS) measurement is twice the standard error on the RV (σ_{RV}).

WASP-119				
WASP-	BJD(UTC) – 2 400 000	RV (km s ⁻¹)	σ_{RV} (km s ⁻¹)	BS (km s ⁻¹)
119	56548.906910	8.45864	0.01532	-0.09451
119	56570.857181	8.24473	0.01756	0.01842
119	56575.777466	8.24146	0.01258	0.01012
119	56593.863562	8.42141	0.02158	-0.00951
119	56622.794968	8.33225	0.02814	-0.05036

2011), and the CORALIE spectrograph and EulerCam photometer (Lendl et al. 2012) on the Swiss Euler 1.2-m telescope at La Silla. We find that about 1-in-12 candidates turns out to be a planet, the remainder being blends that are unresolved in the WASP images (which have 14 arcsec pixels) or astrophysical transit mimics, usually eclipsing binary stars. A list of observations reported in this paper is given in Table 1. The light curve data used in our analysis are given in Table 2 and the radial velocities measured from the CORALIE spectra are listed in Table 3. The radial velocity measurements presented in Table 3 use a mask based on a G2-type template for the calculation of the cross-correlation function. We also measured the radial velocity using a K5-type template and found that the results are consistent to within 7 m s⁻¹. This test excludes most scenarios in which the periodic RV variations we observe are due to an eclipsing binary star blended with the light of the target star (Huélamo et al. 2008). Also given in Table 3 are the bisector span (BS) measurements that characterise the asymmetry in the stellar line profiles for each spectrum (Queloz et al. 2001). The bisector span will show a significant correlation with the measured radial velocity (RV) if the apparent variations in RV are due to stellar magnetic activity (star spots) or blended spectra in a multiple star system. We used the Bayesian information criterion (BIC) to test the significance of any correlation between RV and BS for each star, i.e., we calculated the change of BIC going from a constant BS value (weighted mean) to a fit of a straight line to BS as a function of RV. The zero-points of the RV and BS measurements may be slightly different for spectra obtained before or after the upgrade to CORALIE in November 2014 so we analysed data either side of this date independently. Weak evidence for a correlation is present in the data obtained prior to the CORALIE upgrade for WASP-124 (BIC decreased by 6.6) but this apparent correlation is not confirmed by the data obtained post-upgrade and there is no other indication that WASP-124 is an active star

Table 4. Stellar parameters. The V magnitude is based on the estimated apparent Gaia G magnitude from Smart (2013) and the transformation V–G from Jordi et al. (2010) assuming $V-I_C \approx 0.7$ for all stars. Other symbols are defined in the text. The 1SWASP identifier provides the J2000.0 coordinates of the star taken from the USNO-B1.0 catalogue (Monet et al. 2003).

Parameter	Value
WASP-119	
Identifiers	1SWASP J034343.96–651137.8 2MASS 03434402–6511378
Spectral type	G5
V	12.2 ± 0.4
T_{eff} (K)	5650 ± 100
$\log g$ (cgs)	4.5 ± 0.3
$v \sin I$ (km s ^{−1})	0.7 ± 0.9
[Fe/H]	$+0.14 \pm 0.10$
$\log A(\text{Li})$	1.36 ± 0.10
WASP-124	
Identifiers	1SWASP J221051.43–304458.3 2MASS 22105143–3044588
Spectral type	F9
V	12.7 ± 0.4
T_{eff} (K)	6050 ± 100
$\log g$ (cgs)	4.0 ± 0.25
$v \sin I$ (km s ^{−1})	3.2 ± 0.9
[Fe/H]	-0.02 ± 0.11
$\log A(\text{Li})$	2.67 ± 0.08
WASP-126	
Identifiers	1SWASP J041329.75–691336.6 TYC 9153-833-1 2MASS 04132972–6913365
Spectral type	G2
V	10.8 ± 0.5
T_{eff} (K)	5800 ± 100
$\log g$ (cgs)	4.4 ± 0.25
$v \sin I$ (km s ^{−1})	0.5 ± 0.5
[Fe/H]	$+0.17 \pm 0.08$
$\log A(\text{Li})$	1.18 ± 0.09
WASP-129	
Identifiers	1SWASP J114511.75–420350.3 TYC 7749-508-1 2MASS 11451175–4203501
Spectral type	G1
V	12.3 ± 0.6
T_{eff} (K)	5900 ± 100
$\log g$ (cgs)	4.1 ± 0.25
$v \sin I$ (km s ^{−1})	2.7 ± 0.6
[Fe/H]	$+0.15 \pm 0.09$
$\log A(\text{Li})$	2.41 ± 0.09
WASP-133	
Identifiers	1SWASP J205818.07–354747.6 2MASS 20581808–3547475
Spectral type	G4
V	12.9 ± 0.4
T_{eff} (K)	5700 ± 100
$\log g$	4.1 ± 0.25
$v \sin I$ (km s ^{−1})	0.3 ± 0.7
[Fe/H]	$+0.29 \pm 0.12$
$\log A(\text{Li})$	2.67 ± 0.09

or a multiple star system, so we assume that this correlation is a statistical fluke. None of the data sets for any other stars show any evidence for a correlation between BS and RV.

To measure precise planetary radii, we obtained follow-up photometry of the transits of these stars with EulerCam and TRAPPIST. The dates of observation and filters used are given in Table 1. The NGTS filter on the EulerCam instrument has a central wavelength of 698 nm and the effective bandwidth is 312 nm. The ExoPlanet-BB filter manufactured by Astrodon blocks wavelengths below about 500 nm. The NIR filter is an NIR luminance filter also from Astrodon that blocks light below 700 nm.

3. The host stars

3.1. Spectroscopic analysis

The CORALIE spectra of the host stars were co-added to produce spectra for analysis using the methods described in Gillon et al. (2009) and Doyle et al. (2013). We used the H α line to estimate the effective temperature (T_{eff}), and the Na I D and Mg I b lines as diagnostics of the surface gravity ($\log g$). The resulting parameters are listed in Table 4. The CORALIE spectra do not have a sufficient number of clean spectral lines to determine reliable values for [Mg/Fe] or [Na/Fe] independently of $\log g$ so the quoted error in $\log g$ includes an additional 0.15 dex error due to the unknown Mg abundance of these stars (Brewer et al. 2015). The iron abundances were determined from equivalent-width measurements of several clean and unblended Fe I lines and are given relative to the solar value presented in Asplund et al. (2009). The quoted abundance errors include that given by the uncertainties in T_{eff} and $\log g$, as well as the scatter due to measurement and atomic data uncertainties. The projected rotation velocities ($v \sin I$) were determined by fitting the profiles of the Fe I lines after convolving with the CORALIE instrumental resolution ($R = 55\,000$) and a macroturbulent velocity adopted from the calibration of Doyle et al. (2014).

3.2. Rotational modulation

We searched the WASP photometry of each star for rotational modulations by using a sine-wave fitting algorithm as described by Maxted et al. (2011). We estimated the significance of periodicities by subtracting the fitted transit light curve and then repeatedly and randomly permuting the nights of observation. For none of our stars was a significant periodicity obtained, with 95%-confidence upper limits on the semi-amplitude being typically 1 mmag.

4. System parameters

The CORALIE radial-velocity measurements were combined with the WASP, EulerCam and TRAPPIST photometry in a simultaneous Markov-chain Monte-Carlo (MCMC) analysis to find the system parameters. For details of our methods see Collier Cameron et al. (2007). Limb-darkening was parameterised using the 4-parameter non-linear law and coefficients from Claret (2000). The value of T_{eff} used to interpolate the limb darkening coefficients from these tables is a free parameter in the fit but is constrained by a Gaussian prior according to value of T_{eff} and its standard error for each star from Table 4. The resulting values of T_{eff} are all found to be consistent with prior values so we do not quote them here. We used the coefficients for the R-band to model the WASP light curves and

those obtained with the ExoPlanet-BB, NGTS and Gunn R filters. For the z' and NIR filters we used the coefficients for the Sloan z' -band from Claret (2004). The coefficients for $\log g=4.5$, $[M/H]=0.1$ and micro-turbulence velocity $V_T = 2 \text{ km s}^{-1}$ were interpolated from these tables for each trial value of the effective temperature in the MCMC chain. Changing the choice of table used to calculate the limb darkening coefficients assigned to these non-standard filters from z' to R-band or from R-band to I-band changes the mass and radius derived for the stars and planets by less than the quoted uncertainty. For TRAPPIST observations where a meridian flip was required the data obtained with the telescope on the west side and east side of the German equatorial mount were analysed independently to allow for any change in the photometric zero-point. To account for stellar noise in the radial velocity measurements (“jitter”) we used a circular orbit fit by least-squares with the orbital period and time of mid-transit fixed to values determined from the photometry. We then used trial-and-error to find the amount of jitter required to achieve a reduced χ^2 value of 1 when this additional variance is added in quadrature to the standard errors given in Table 3. The values of the jitter (σ_{jit}) used in our analysis are given in Table 6. We did not find strong evidence in any of these systems for a linear drift in the apparent centre-of-mass velocity, $\frac{dy}{dt}$. There is weak evidence for a drift in the velocity of WASP-126 A ($\frac{dy}{dt} = (5.5 \pm 3.0) \times 10^{-5} \text{ km s}^{-1} \text{ d}^{-1}$), but we do not consider this to be a significant detection. Adding this extra parameter in the modelling of the data changes the other parameters by less than one standard deviation.

For all of our planets the data are compatible with zero eccentricity and hence we imposed a circular orbit – the rationale for this assumption is discussed in Anderson et al. (2012). The fitted parameters were thus T_c , P , ΔF , T_{14} , b , K_1 , where T_c is the epoch of mid-transit, P is the orbital period, ΔF is the planet-star area ratio (i.e., the fractional flux-deficit that would be observed during transit in the absence of limb-darkening), T_{14} is the total transit duration (from first to fourth contact), b is the impact parameter of the planet’s path across the stellar disc, and K_1 is the stellar reflex velocity semi-amplitude.

The analysis of the transit light curves leads directly to an estimate of the stellar density (Seager & Mallén-Ornelas 2003) and the spectroscopic orbit can then be used to infer the planetary surface gravity (Southworth et al. 2007). One additional constraint is required to obtain the masses and radii of the star and planet. The additional constraint we have used is the mass of the star estimated using stellar models based on the effective temperature, metallicity and mean density of the star. We used the open source software BAGEMASS¹ to calculate the posterior mass distribution for each star using the Bayesian method described by Maxted et al. (2015a). The models used in BAGEMASS were calculated using the GARSTEC stellar evolution code (Weiss & Schlattl 2008). The mean and standard deviation of the posterior mass distribution for the star are included in the MCMC analysis as a Gaussian prior. The mass and age of the stars derived are shown in Table 5. There is no good match to the observed density of WASP-129 A if we use the standard grid of stellar models in BAGEMASS with the following linear relation between helium abundance, Y and heavy element abundance, Z : $Y = 0.2485 + 0.984Z$, where the zero-point in this relation is the primordial helium abundance (Steigman 2010) and the gradient is set to match the current solar helium abundance. For this star we used the grid of stellar models provided within bagemass with an enhanced initial helium abundance ($\Delta Y = +0.02$). This

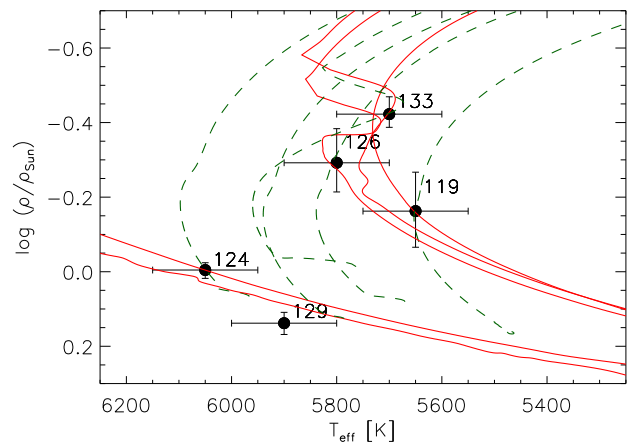


Fig. 1. Planet host stars in the T_{eff} – density plane (error bars labelled by WASP identification number) compared to best-fit evolution tracks (dashed lines) and isochrones (solid lines) for the masses and ages listed in Table 5 assuming $[\text{Fe}/\text{H}]$ as listed in Table 4.

Table 5. Stellar mass and age estimates. The mean and standard deviation of the posterior distributions are given together with the best-fit values in parentheses.

Star	Mass [M_{\odot}]	Age [Gyr]
WASP-119 A	1.02 ± 0.06 (1.01)	8.0 ± 2.5 (8.1)
WASP-124 A	1.07 ± 0.05 (1.10)	2.1 ± 1.4 (1.1)
WASP-126 A	1.12 ± 0.06 (1.10)	6.4 ± 1.6 (6.4)
WASP-129 A ^a	1.00 ± 0.03 (1.03)	1.0 ± 0.9 (0.0)
WASP-133 A	1.16 ± 0.08 (1.20)	6.8 ± 1.8 (5.7)

Notes. ^(a) Values for helium-enhanced models, $\Delta Y = +0.02$

has the effect of reducing the mass estimate for this star by about one standard deviation. The best-fit stellar evolution tracks and isochrones are shown in Fig. 1.

The parameters for each planetary system derived from our analysis are given in Table 6. The discovery data and model fits to these observations are shown in Figs. 2 – 6.

4.1. Kinematics

The kinematics of our sample in Galactic coordinates are summarized in Table 7. The proper motions are taken from Smart (2013) and the radial velocities are from Table 6. To calculate the distance we use the apparent K_s -band magnitude from Skrutskie et al. (2006), the radius of the star from Table 6 and the angular diameter of the star based on the calibration of K -band surface brightness – effective temperature relation from Kervella et al. (2004). We assume that interstellar reddening is negligible and that $K = K_s + 0.044$ (Bessell 2005). The transformation of these variables to Galactic (U , V , W) velocity in the local standard of rest is done using the procedure `gal_uvw`.² U is positive towards the Galactic anti-centre and the solar motion is taken from Coşkunoğlu et al. (2011).

Holmberg et al. (2007) find that individual stars in the solar neighbourhood cannot be unambiguously assigned to different populations based only on their kinematics, but the well-defined age – velocity dispersion relation for solar-type stars does suggest that WASP-126 A is likely to be older than about 4 Gyr

¹ <http://sourceforge.net/projects/bagemass>

² `idlastro.gsfc.nasa.gov`

Table 6. System parameters. The UTC time of mid-transit, T_c , is given as HJD–2450000. Upper limits on the eccentricity, e , are 95% confidence limits. Values in parantheses are standard errors in the final digit. T_{eq} is the planet equilibrium temperature assuming zero albedo. Where two values of the jitter (σ_{jit}) are given, these apply to radial velocity measurements taken before and after the upgrade to the CORALIE spectrograph, respectively.

Parameter	WASP-119	WASP-124	WASP-126	WASP-129	WASP-133
P (d)	2.49979(1)	3.372650(1)	3.28880(1)	5.748145(4)	2.176423(1)
T_c	6537.547(2)	7028.5834(1)	6890.3191(6)	7027.4373(2)	7116.9874(2)
T_{14} (d)	0.126 ± 0.006	0.1071 ± 0.0006	0.142 ± 0.002	0.1119 ± 0.0008	0.1433 ± 0.0007
ΔF	0.0131 ± 0.0008	0.0154 ± 0.0002	0.0061 ± 0.0002	0.0114 ± 0.0001	0.0074 ± 0.0001
b	$0.50^{+0.10}_{-0.24}$	0.61 ± 0.02	0.3 ± 0.2	0.62 ± 0.02	0.2 ± 0.1
i ($^\circ$)	85 ± 2	86.3 ± 0.2	87.9 ± 1.5	87.7 ± 0.2	87 ± 1
R_*/a	0.158 ± 0.015	0.106 ± 0.018	$0.131^{+0.011}_{-0.004}$	0.066 ± 0.0017	$0.194^{+0.006}_{-0.003}$
K_1 (km s $^{-1}$)	0.181 ± 0.010	0.077 ± 0.008	0.036 ± 0.005	0.11 ± 0.01	0.17 ± 0.01
γ (km s $^{-1}$)	8.404 ± 0.007	-5.876 ± 0.006	29.164 ± 0.004	21.988 ± 0.008	-23.913 ± 0.009
M_* (M_\odot)	1.02 ± 0.06	1.07 ± 0.05	1.12 ± 0.06	1.00 ± 0.03	1.16 ± 0.08
R_* (R_\odot)	1.2 ± 0.1	1.02 ± 0.02	$1.27^{+0.10}_{-0.05}$	0.90 ± 0.02	1.44 ± 0.05
$\log g_*$ (cgs)	4.26 ± 0.08	4.44 ± 0.02	$4.28^{+0.03}_{-0.07}$	4.53 ± 0.02	4.18 ± 0.02
ρ_* (ρ_\odot)	0.54 ± 0.18	0.99 ± 0.05	$0.56^{+0.06}_{-0.12}$	1.38 ± 0.10	0.39 ± 0.03
M_P (M_{Jup})	1.23 ± 0.08	0.60 ± 0.07	0.28 ± 0.04	1.0 ± 0.1	1.16 ± 0.09
R_P (R_{Jup})	1.4 ± 0.2	1.24 ± 0.03	$0.96^{+0.10}_{-0.05}$	0.93 ± 0.03	1.21 ± 0.05
$\log g_P$ (cgs)	3.2 ± 0.1	2.95 ± 0.05	2.83 ± 0.09	3.42 ± 0.05	3.26 ± 0.04
ρ_P (ρ_J)	0.5 ± 0.2	0.32 ± 0.04	0.31 ± 0.08	1.2 ± 0.2	0.66 ± 0.07
a (AU)	0.0363 ± 0.0007	0.0449 ± 0.0007	0.0449 ± 0.0008	0.0628 ± 0.0007	0.0345 ± 0.0007
e	< 0.058	< 0.017	< 0.18	< 0.096	< 0.17
T_{eq} (K)	1600 ± 80	1400 ± 30	1480 ± 60	1100 ± 25	1790 ± 40
σ_{jit} (km s $^{-1}$)	0.0225, 0.0205	0.0115, 0	0.062, 0.014	0.0165	0

Table 7. Kinematics and distances. Proper motions are from Smart (2013).

Star	μ_α [mas/yr]	μ_δ [mas/yr]	d [pc]	U [km s $^{-1}$]	V [km s $^{-1}$]	W [km s $^{-1}$]
WASP-119	22.1 ± 2.1	16.0 ± 1.8	333 ± 29	28 ± 4	-10 ± 3	12 ± 3
WASP-124	-2.0 ± 1.3	-14.4 ± 1.0	433 ± 11	-16 ± 2	-16 ± 2	12 ± 2
WASP-126	62.0 ± 1.1	52.9 ± 0.9	234 ± 15	64 ± 5	-47 ± 3	14 ± 2
WASP-129	11.8 ± 1.3	0.7 ± 1.8	246 ± 7	-27 ± 2	-0 ± 1	18 ± 2
WASP-133	9.3 ± 1.5	-7.8 ± 1.0	547 ± 21	24 ± 3	-8 ± 3	2 ± 3

based on its kinematics, consistent with the age of about 6 Gyr we have derived using stellar models.

5. Discussion

WASP-119 is a typical hot Jupiter system in terms of the mass ($1.2 M_{\text{Jup}}$), radius ($1.3 R_{\text{Jup}}$) and orbital period (2.5 d) of the planet. The host star has a similar mass to the Sun but appears to be much older based on its effective temperature and density (Fig. 1).

WASP-124 is also a typical hot Jupiter system ($0.6 M_{\text{Jup}}$, $1.2 R_{\text{Jup}}$, 3.4 d) but with an apparently much younger host star, although not so young that it has an enhanced lithium abundance. The projected rotation velocity of WASP-124 A is one of the largest in our sample ($v \sin I \approx 3 \text{ km s}^{-1}$). Rapid rotation is expected for young solar-type stars, but it is unclear whether the age estimates for planet host stars based on their rotation rate (gyrochronological ages) are reliable (Maxted et al. 2015b).

WASP-126 A is the brightest star presented here and also hosts the lowest-mass planet in our sample ($0.3 M_{\text{Jup}}$). The radius of this planet is quite large ($0.95 R_{\text{Jup}}$) so it also has the lowest surface gravity of these newly-discovered planets. This combination of low surface gravity (i.e., large atmospheric scale

height) and a bright host star make this a good target for transmission spectroscopy.

The high density of WASP-129 A can be explained using stellar models with enhanced initial helium abundance. The helium-enhanced models we have used here ($\Delta Y = +0.02$) provide an adequate fit to the observed properties of this star, so we expect that models with an even higher helium abundance ($\Delta Y \approx +0.04$) would provide a much better fit. Maxted et al. (2015b) found similarly high densities for two other hot Jupiter host stars (HAT-P-11 A and WASP-84 A). These high densities inferred from the transit light curves cannot be explained by contamination of the light curve by a third star in the system since this would lead to a shallower eclipse depth and a lower inferred value for the stellar density (Seager & Mallén-Ornelas 2003). The distribution of the initial helium abundance for solar-type stars is very uncertain since there is no direct way to measure the helium abundance of cool stars, so it is unclear how this parameter impacts on our understanding of the age and mass distributions for planet host stars. The surface gravity of WASP-129 A derived from our analysis of the light curves and spectroscopic orbit (4.53 ± 0.02) is clearly inconsistent with the value derived from our analysis of its spectrum (4.1 ± 0.1). Analysis of the spectrum of WASP-129 A at high resolution and higher signal-to-noise may help to find the reason for this discrepancy.

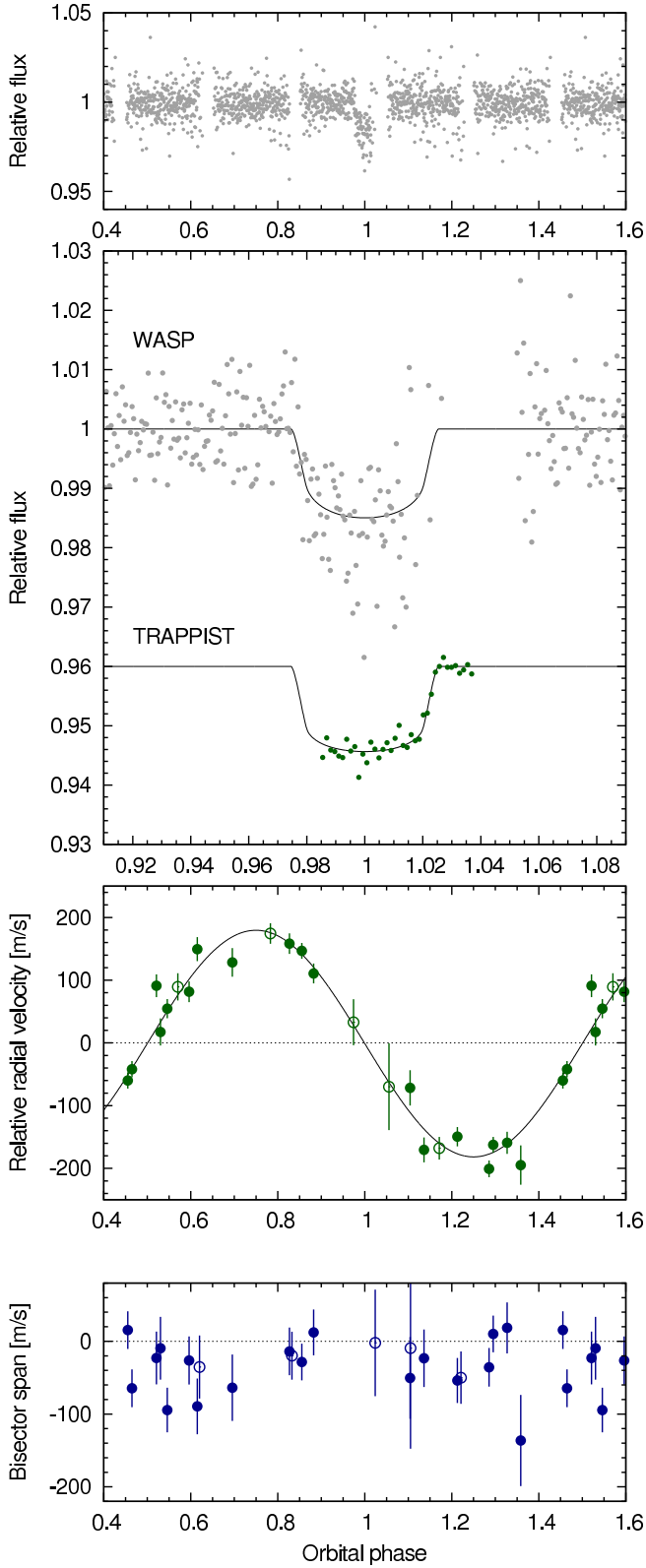


Fig. 2. WASP-119 b discovery data: (Top) The WASP-South light curve folded on the transit period. (Second panel) The binned WASP data with (offset) the follow-up transit light curves (ordered from top-to-bottom as in Table 1) together with the fitted MCMC model. (Third) The CORALIE radial velocities with the fitted model. Filled/open symbols denote data obtained before/after the upgrade to the CORALIE spectrograph, respectively. (Lowest) The bisector spans; the absence of any significant correlation with radial velocity is a check against transit mimics.

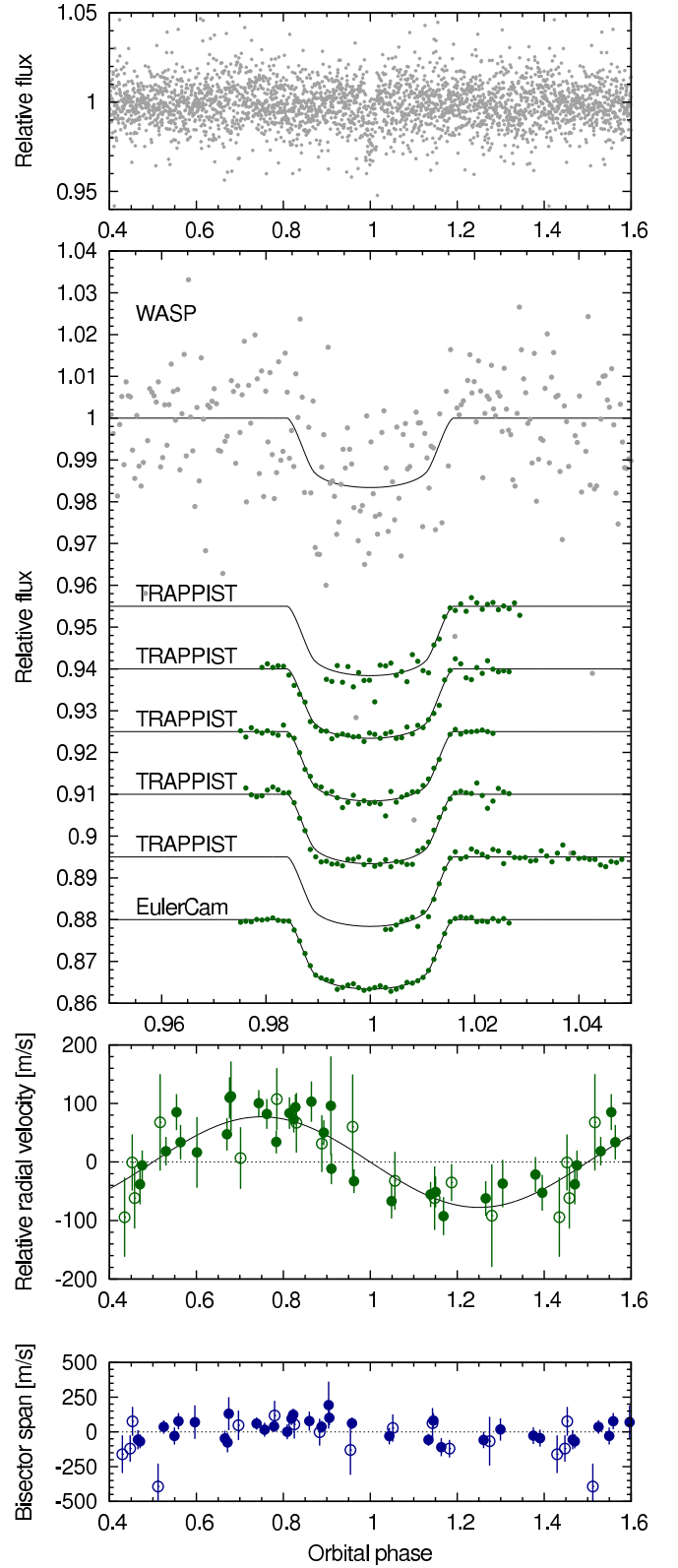


Fig. 3. WASP-124 b discovery data, as for Fig 1.

WASP-129 b has a slightly longer orbital period than most hot Jupiters (5.7 d) and, for the stellar mass that we have adopted, also has a smaller radius ($0.9 R_{\text{Jup}}$) than most hot Jupiters with similar masses ($1.0 M_{\text{Jup}}$). The high density estimate for WASP-129 b implied by these parameters should be treated with some caution until the mass of the host star can be determined with

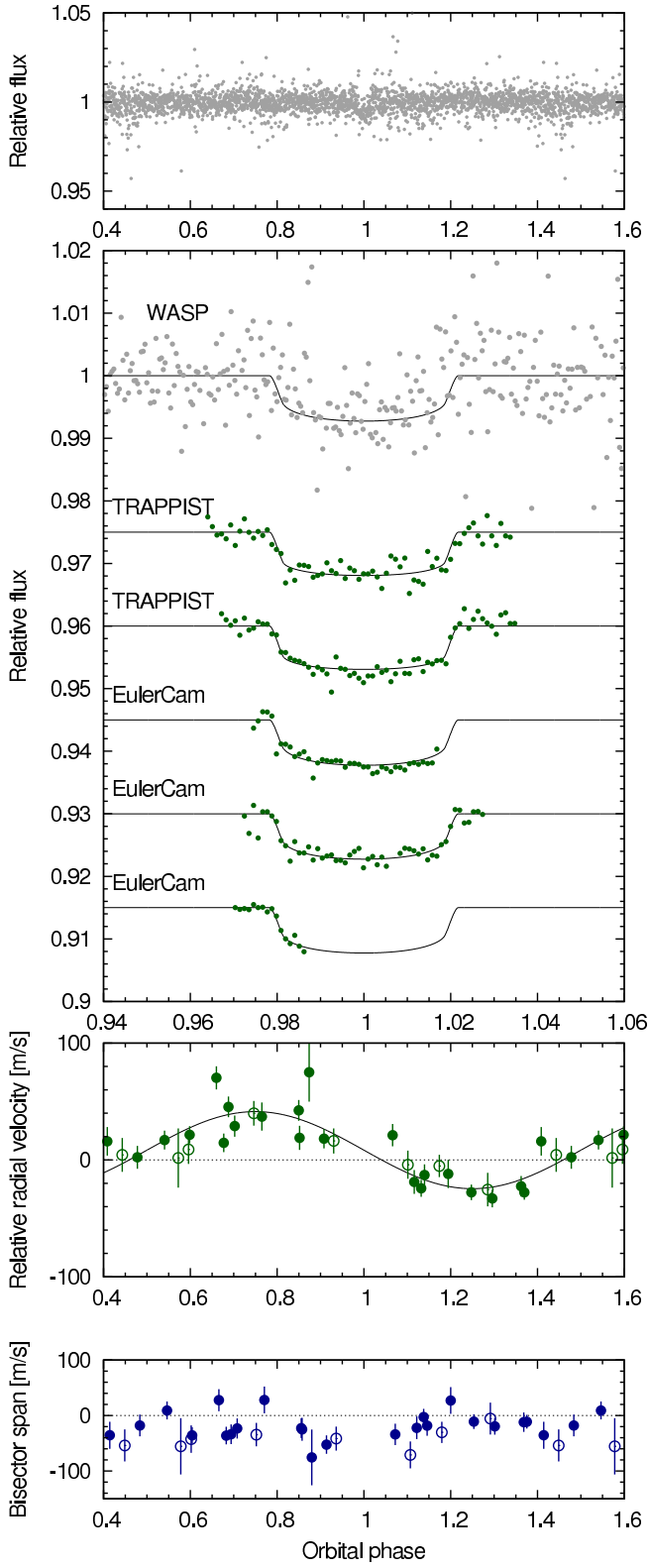


Fig. 4. WASP-126 b discovery data, as for Fig 1. The measured drift in the centre-of-mass velocity given in Table 6 has been subtracted from the radial velocities prior to plotting.

greater confidence. The surface gravity of this planet is also high compared to other hot Jupiters and this quantity is independent of the assumed stellar mass.

WASP-133 A appears to be an old, metal-rich G-dwarf when compared to stellar evolution models (Fig. 1). WASP-133 b is

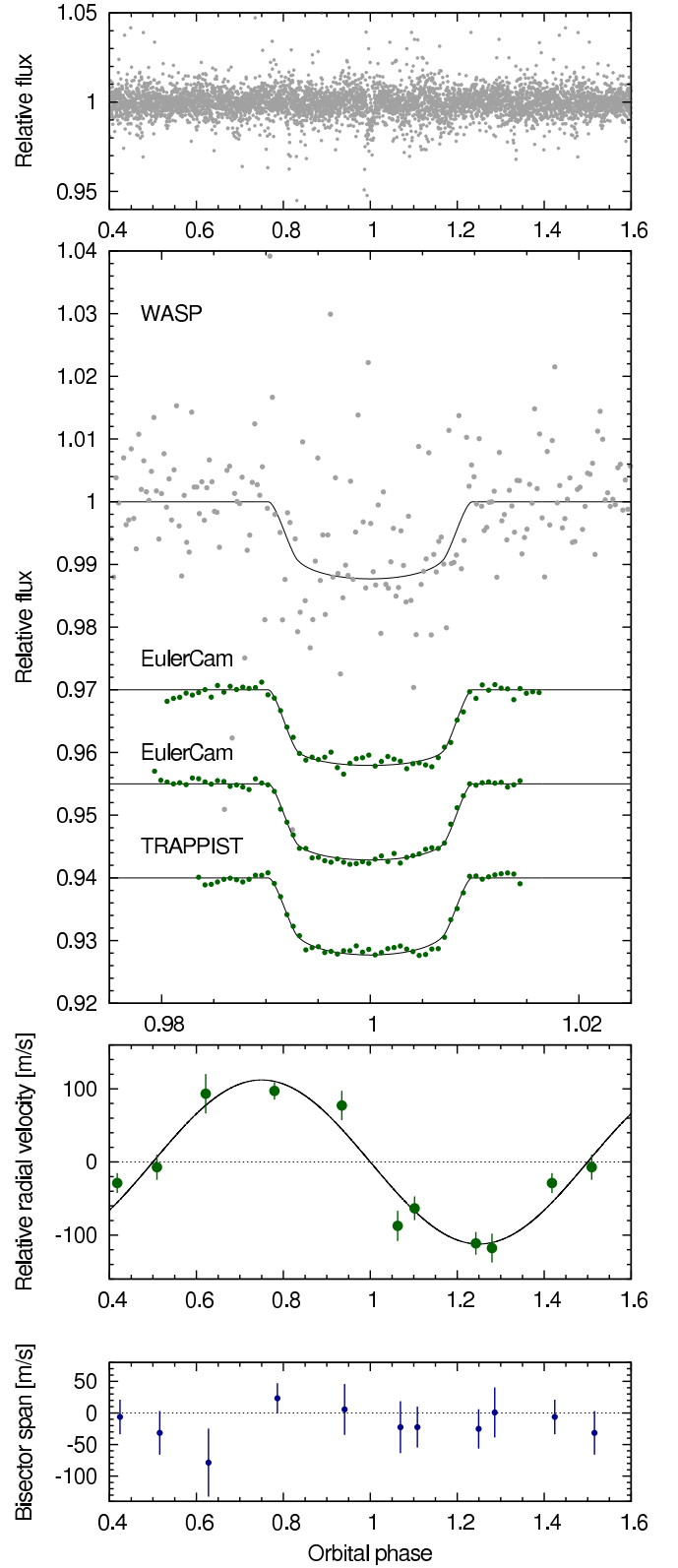


Fig. 5. WASP-129 b discovery data, as for Fig 1.

a hot Jupiter ($1.2 M_{\text{Jup}}$, $1.2 R_{\text{Jup}}$) with the shortest orbital period of the systems presented here (2.2 d). The surface lithium abundance of WASP-133 A ($A(\text{Li})=2.7$) is significantly higher than other stars of similar age and effective temperature ($A(\text{Li}) < 2.5$, Sestito & Randich 2005). This is a counter-example of the general trend for planet host stars to be depleted in lithium

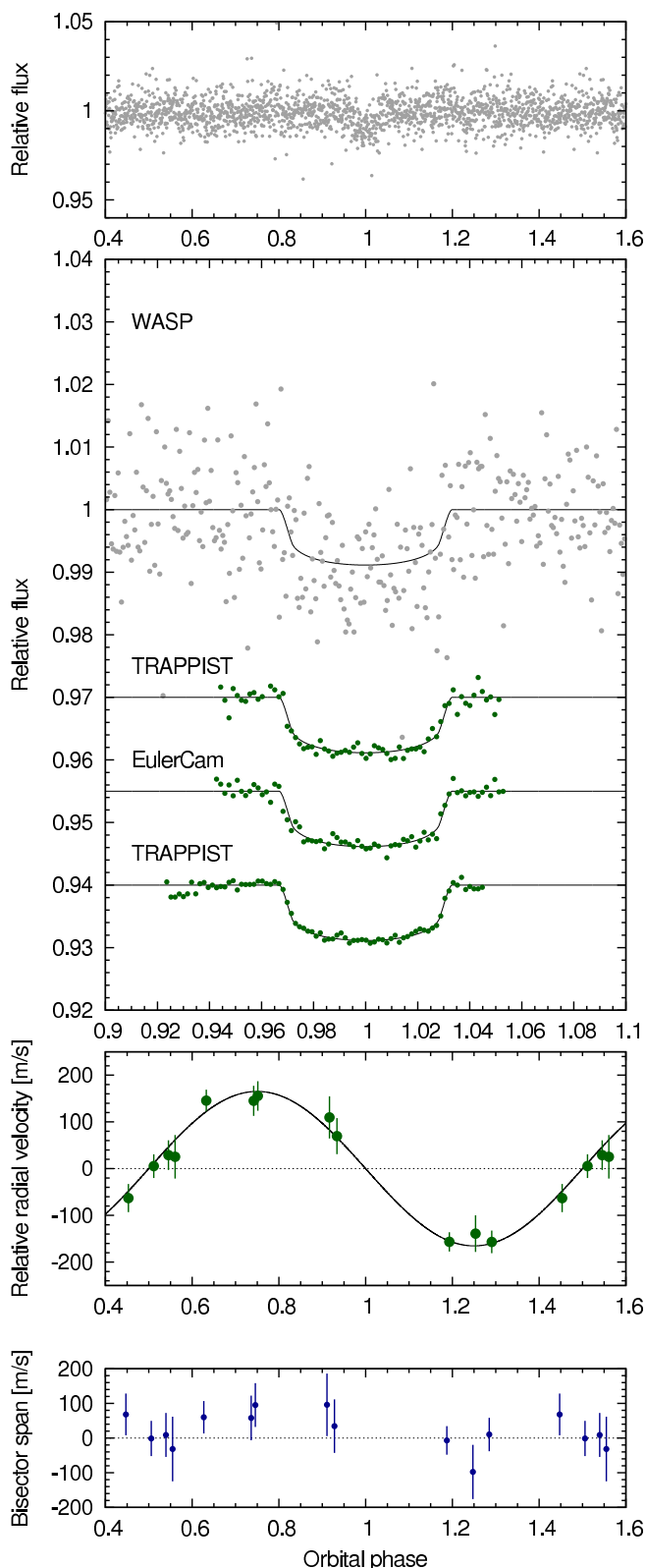


Fig. 6. WASP-133 b discovery data, as for Fig 1.

compared to similar non-planet host stars (Maxted et al. 2010; Gonzalez 2015; Deal et al. 2015). Whether this anomaly is connected to the slow rotation of this star or some other factor is difficult to ascertain from the consideration of a single system. Understanding the relationships between these different properties of planets and their host star can only be done by studying

a large sample of planetary systems, such as the one being compiled using WASP-South of which these new discoveries are the latest contribution.

Acknowledgements

WASP-South is hosted by the South African Astronomical Observatory and we are grateful for their ongoing support and assistance. Funding for WASP comes from consortium universities and from the UK's Science and Technology Facilities Council. TRAPPIST is funded by the Belgian Fund for Scientific Research (Fond National de la Recherche Scientifique, FNRS) under the grant FRFC 2.5.594.09.F, with the participation of the Swiss National Science Foundation (SNF). M. Gillon and E. Jehin are FNRS Research Associates. The authors thank the anonymous referee for helpful comments which have improved the quality of this paper.

References

- Anderson, D. R., Collier Cameron, A., Gillon, M., et al. 2012, *MNRAS*, 422, 1988
- Asplund, M., Grevesse, N., Sauval, A. J., & Scott, P. 2009, *ARA&A*, 47, 481
- Bakos, G., Noyes, R. W., Kovács, G., et al. 2004, *PASP*, 116, 266
- Bakos, G. Á., Csabry, Z., Penev, K., et al. 2013, *PASP*, 125, 154
- Becker, J. C., Vanderburg, A., Adams, F. C., Rappaport, S. A., & Schwengeler, H. M. 2015, *ApJ*, 812, L18
- Bessell, M. S. 2005, *ARA&A*, 43, 293
- Brewer, J. M., Fischer, D. A., Basu, S., Valenti, J. A., & Piskunov, N. 2015, *ApJ*, 805, 126
- Claret, A. 2000, *A&A*, 363, 1081
- Claret, A. 2004, *A&A*, 428, 1001
- Coşkunoglu, B., Ak, S., Bilir, S., et al. 2011, *MNRAS*, 412, 1237
- Collier Cameron, A., Bouchy, F., Hébrard, G., et al. 2007, *MNRAS*, 375, 951
- Deal, M., Richard, O., & Vauclair, S. 2015, *A&A*, 584, A105
- Doyle, A. P., Davies, G. R., Smalley, B., Chaplin, W. J., & Elsworth, Y. 2014, *MNRAS*, 444, 3592
- Doyle, A. P., Smalley, B., Maxted, P. F. L., et al. 2013, *MNRAS*, 428, 3164
- Gillon, M., Jehin, E., Magain, P., et al. 2011, in *European Physical Journal Web of Conferences*, Vol. 11, *European Physical Journal Web of Conferences*, 06002
- Gillon, M., Smalley, B., Hebb, L., et al. 2009, *A&A*, 496, 259
- Gonzalez, G. 2015, *MNRAS*, 446, 1020
- Holmberg, J., Nordström, B., & Andersen, J. 2007, *A&A*, 475, 519
- Howell, S. B., Sobek, C., Haas, M., et al. 2014, *PASP*, 126, 398
- Huélamo, N., Figueira, P., Bonfils, X., et al. 2008, *A&A*, 489, L9
- Jehin, E., Gillon, M., Queloz, D., et al. 2011, *The Messenger*, 145, 2
- Jordi, C., Gebran, M., Carrasco, J. M., et al. 2010, *A&A*, 523, A48
- Kervella, P., Thévenin, F., Di Folco, E., & Ségransan, D. 2004, *A&A*, 426, 297
- Lendl, M., Anderson, D. R., Collier-Cameron, A., et al. 2012, *A&A*, 544, A72
- Maxted, P. F. L., Anderson, D. R., Collier Cameron, A., et al. 2010, *PASP*, 122, 1465
- Maxted, P. F. L., Anderson, D. R., Collier Cameron, A., et al. 2011, *PASP*, 123, 547
- Maxted, P. F. L., Serenelli, A. M., & Southworth, J. 2015a, *A&A*, 575, A36
- Maxted, P. F. L., Serenelli, A. M., & Southworth, J. 2015b, *A&A*, 577, A90
- Monet, D. G., Levine, S. E., Canzian, B., et al. 2003, *AJ*, 125, 984
- Neveu-VanMalle, M., Queloz, D., Anderson, D. R., et al. 2015, *A&A*, in press (arXiv:1509.07750)
- Pepper, J., Stanek, K. Z., Pogge, R. W., et al. 2008, *AJ*, 135, 907
- Pollacco, D., Skillen, I., Collier Cameron, A., et al. 2008, *MNRAS*, 385, 1576
- Pollacco, D. L., Skillen, I., Collier Cameron, A., et al. 2006, *PASP*, 118, 1407
- Queloz, D., Henry, G. W., Sivan, J. P., et al. 2001, *A&A*, 379, 279
- Rauer, H. et al. 2014, *Experimental Astronomy*, 38, 249
- Ricker, G. R. et al. 2015, *Journal of Astronomical Telescopes, Instruments, and Systems*, 1, 014003
- Seager, S. & Mallén-Ornelas, G. 2003, *ApJ*, 585, 1038
- Sestito, P. & Randich, S. 2005, *A&A*, 442, 615
- Skrutskie, M. F. et al. 2006, *AJ*, 131, 1163
- Smart, R. L. 2013, *VizieR Online Data Catalog*, 1324
- Southworth, J., Wheatley, P. J., & Sams, G. 2007, *MNRAS*, 379, L11
- Steigman, G. 2010, *J. Cosmology and Astroparticle Phys.*, 4, 29
- Weiss, A. & Schlattl, H. 2008, *Ap&SS*, 316, 99